Predicting Solar Disturbance Effects on Navigation Systems

M. Lockwood, M. N. Wild, R. Stamper, C. J. Davis and M. Grande

(*World Data Centre*, *Rutherford Appleton Laboratory*)

A variety of operational systems are vulnerable to disruption by solar disturbances brought to the Earth by the solar wind. Of particular importance to navigation systems are energetic charged particles which can generate temporary malfunctions and permanent damage in satellites. Modern spacecraft technology may prove to be particularly at risk during the next maximum of the solar cycle. In addition, the associated ionospheric disturbances cause phase shifts of transionospheric and ionosphere-reflected signals, giving positioning errors and loss of signal for GPS and Loran-C positioning systems and for over-the-horizon radars. We now have sufficient understanding of the solar wind, and how it interacts with the Earth's magnetic field, to predict statistically the likely effects on operational systems over the next solar cycle. We also have a number of advanced ways of detecting and tracking these disturbances through space but we cannot, as yet, provide accurate forecasts of individual disturbances that could be used to protect satellites and to correct errors. In addition, we have recently discovered long-term changes in the Sun, which mean that the number and severity of the disturbances to operational systems are increasing.

1. SOLAR-TERRESTRIAL PHYSICS. The Sun emits a stream of ionised gas (*plasma*) called the *solar wind*, which impacts upon the Earth's *geomagnetic field*. Although this flow is continuous, it is highly variable in both its flux and speed. The geomagnetic field deflects most of the energy associated with the solar wind away from the Earth, leaving a low-density cavity called the *magnetosphere*. However, a small fraction of incident energy is extracted by the magnetosphere because of a process called *magnetic reconnection*. Reconnection interconnects the geomagnetic field with a weak magnetic field of solar origin, called the *interplanetary magnetic field* (IMF), which is dragged to Earth by the solar wind flow. This process works best with antiparallel magnetic fields and, because the geomagnetic field presents a northward field to the solar wind flow, the fraction of the incident energy that is extracted by the magnetosphere is much greater when the IMF points southward [see review by Lockwood, 1997]. The average power density of the solar wind flow is 5×10^{-2} W m^{-2}, which is incident on an area of about 3×10^{16} m^2 presented to the flow by the geomagnetic field. Thus the power incident on the Earth's magnetic field is about $1 \cdot 5 \times 10^{15}$ W and under optimum conditions about 2%, i.e. $\sim 3 \times 10^{13}$ W, is extracted by the magnetosphere. Of this, roughly two thirds is eventually returned to interplanetary space, but the remaining third ($\sim 10^{13}$ W) is deposited in the upper atmosphere (by large-scale currents that flow in the *auroral ovals*) and in the inner magnetosphere (by particle energisation mechanisms). The heating by the auroral currents causes winds and composition changes in the upper atmosphere that propagate around the world. These modulate the rate at which the ionised upper atmosphere (*ionosphere*) is lost and so alter the global distribution of ionospheric
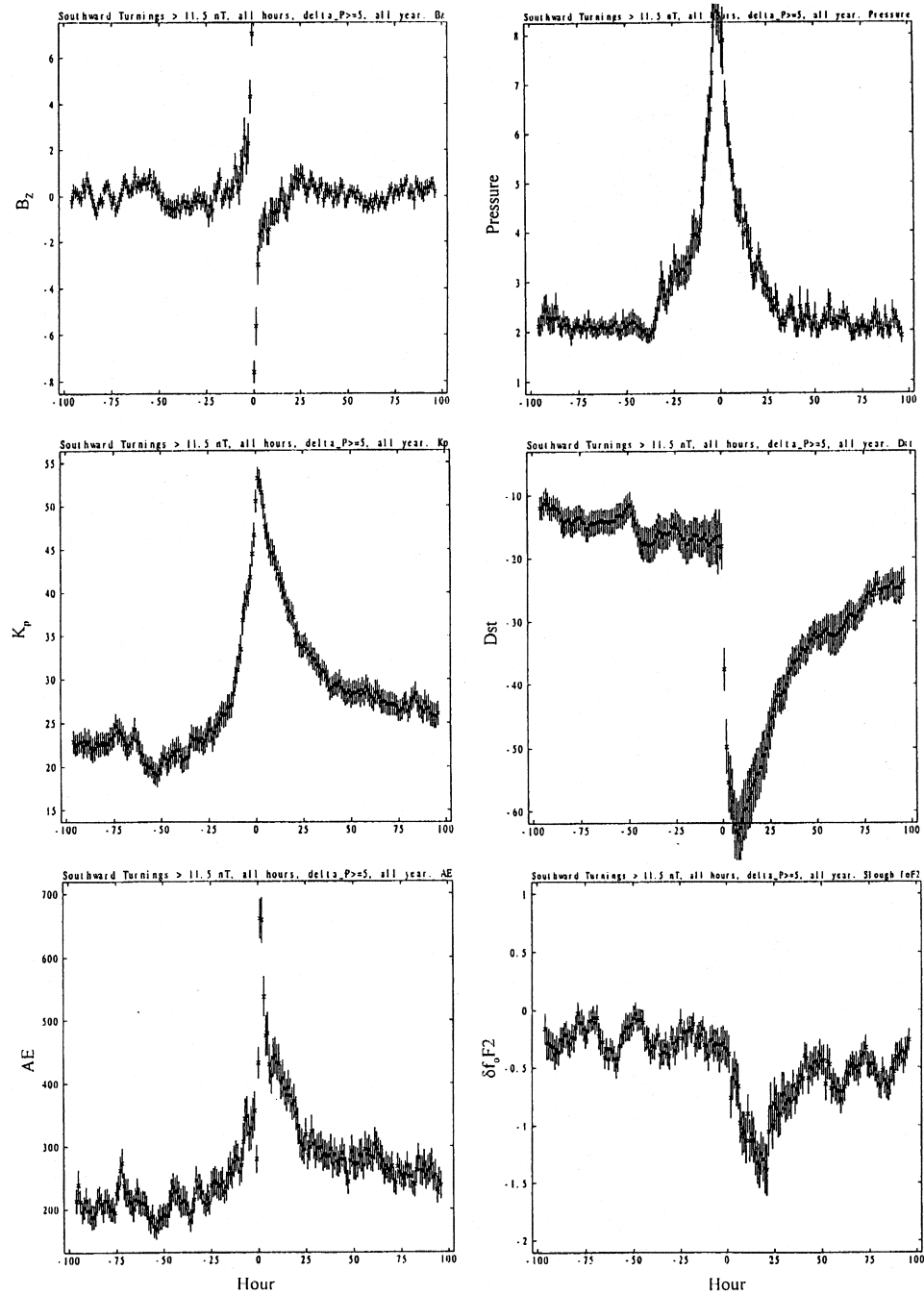
Figure 1. Superposed epoch analysis of the role of the interplanetary magnetic field orientation on geomagnetic and ionospheric disturbances. Each plot shows the means (with error bars of plus and minus one standard deviation) as a function of time relative to a major southward turning of the IMF ($\Delta B_z > 11\cdot5$ nT): (a) IMF B_z; (b) solar wind P_{sw}; (c), (d) and (e) geomagnetic indices Kp, Dst, AE; and (f) foF2 (see text for details) [from Davis et al., 1996].

concentrations and total electron content. The particle acceleration mechanisms cause rises in the fluxes of energetic particles trapped in the geomagnetic field and these particles pose serious dangers to satellites, most of which operate in this region.

A good indicator of the level of energy extraction from the solar wind flow is the level of geomagnetic fluctuations, as quantified using data from ground-based magnetometers by planetary indices such as Ap, Kp and *aa*. We now know a great deal about the various types of solar disturbance and how they lead to geomagnetic activity and the associated effects on the Earth's ionosphere and radiation environment. In particular, the Sun emits massive amounts of material in *Coronal Mass Ejections* (CMEs). Each CME carries of order 10^{13} kg of material (this should be compared with the total mass loss of the Sun by the solar wind which is of order 10^{14} kg per day), typically travelling at 350 km s^{-1} and carrying 10^{24} J of energy. The occurrence of CMEs rises and falls with the 11-year cycle of solar activity, quantified by the number of *sunspots* – slightly cooler and darker regions on the visible disk of the sun. At sunspot minimum, CMEs occur roughly once every four days but this rises to about twice per day at sunspot maximum [Webb and Howard, 1994]. CMEs are emitted in all directions and so only a few impact the earth: roughly speaking, one will hit the Earth every two weeks at sunspot minimum, rising to four per week at sunspot maximum. Events that are travelling toward Earth have a characteristic 'halo' form when seen by an instrument called a *coronograph*. One such event was seen in January 1997 by the LASCO instrument on the SOHO satellite: this was the first time that such a disturbance had been tracked from the Sun all the way to the Earth's ionosphere and inner magnetosphere, allowing a detailed study of its effects [Fox *et al.*, 1998 (and other papers in the same issue); Reeves *et al.*, 1998].

The ejection of CMEs in the direction of the Earth is not yet predictable. When they hit Earth they can give rise to geomagnetic activity which is classed as *non-recurrent* [Joselyn, 1995]. The other major classification geomagnetic disturbance is called *recurrent*. The latter arises because the Earth repeatedly intersects fast streams of solar wind emitted from *coronal holes* in the solar atmosphere that have extended down to near the solar equator (which occurs mainly in the declining phase of the solar cycle) [Wang *et al.*, 1995; Cliver *et al.*, 1996]. These are long-lived and rotate every 25 days, the rotation period near the Sun's equator. However, in 25 days the Earth will have moved almost 25° along its orbit and so it is 27 days before the stream intersects the Earth again and recurrent geomagnetic activity is seen. Both CMEs and fast streams deform the interplanetary medium so, for example, high solar wind densities are seen on the boundaries of fast streams because of a 'snowplough' effect. Some CMEs may well bring with them cooler denser plasma from the solar *photosphere* (the visible solar disk); often this is the remnant of a solar *prominence* associated with the CME. In addition, solar flares near sunspots generate X-rays, which enhance the lower ionosphere, and energetic particles that precipitate into the upper atmosphere near the poles.

The effect that a disturbance has on the Earth depends critically on the orientation of the IMF because this determines the fraction of the incident energy that is extracted from the solar wind and deposited in the Earth's upper atmosphere. If the IMF is northward, the event will buffet the Earth but will then pass harmlessly by. This is not true for southward IMF. Thus the IMF orientation determines the '*geoeffectiveness*' of a solar disturbance. Unfortunately we have no way, as yet, of remotely sensing the IMF orientation in an approaching event. Figure 1 illustrates the

importance of the north–south component of the IMF, by showing the results of a superposed epoch study of 24 years' data from interplanetary space by Davis *et al.* (1996). The centre of the *x*-axis of each plot is time zero, defined as the time that a major southward turning of the IMF impinges on the Earth's magnetosphere, and each point is the average of a parameter (with an error bar of plus and minus one standard deviation) for one-hour intervals relative to that time. The southward turning can be seen in the top left panel (*a*) that shows the northward component of the IMF, B_z (in the Earth's magnetic GSM frame) which becomes negative at time zero. The parameters in the remaining panels are: (*b*) the solar wind dynamic pressure (equivalent to its energy density), $P_{sw} = N_{sw} m_{sw} v_{sw}^2$ (where N_{sw} is the solar wind plasma concentration, m_{sw} is the mean ion mass and v_{sw} is the speed of the solar wind); (*c*) the magnetic Kp index; (*d*) the equatorial Dst index; (*e*) the auroral electrojet (AE) current index and (*f*) the deviation of the ionospheric critical frequency (δfoF2) from its quite time value, as seen at Slough. (The critical frequency foF2 is proportional to the square root of the peak electron concentration in the ionosphere). It can be seen from (*b*) that the CMEs and fast solar wind streams bring a higher energy density P_{sw} to Earth at around the times of southward IMF turnings. The different geomagnetic indices show different responses. The Kp index (*c*) is enhanced by the buffeting by higher-energy solar wind before the southward turning, but is higher after it, whereas the dramatic drop in Dst (*d*) after the southward turning is the signature of enhanced *ring current*, carried by trapped energetic particles injected into the inner magnetosphere. The sharp peak in AE (*e*) immediately after the southward turning is called a *substorm*, an enhancement of the auroral currents that deposit extracted energy in the upper atmosphere. The ionospheric concentrations (*f*) are depressed (negative δfoF2) for one or two days after the southward turning. The responses to the enhanced energy density of the solar wind, and its extraction arising from the southward IMF, are called geomagnetic and ionospheric *storms*.

Solar-terrestrial phenomena cause disruption to a wide variety of operational systems. These range from communications and broadcast systems to oil pipelines and power distribution systems. In the next section, we look at the effects on satellites of the enhanced energetic particle fluxes injected into the inner magnetosphere during a storm. In Section 3, we look at some of the effects of the associated global ionospheric disturbances on radio navigation and positioning systems. In Section 4, we investigate the long-terms trends in these solar-terrestrial phenomena.

2. SATELLITE MALFUNCTIONS. During storms, the energy extracted from the solar wind by the geomagnetic field rises dramatically. Some of this extracted energy increases the fluxes of energetic particles and, in particular, of *highly relativistic electrons* (HREs, sometimes called *killer electrons*). These energetic particles make the environment in which satellites have to operate an extremely hostile one and can give rise to a variety of satellite malfunctions:

(i) *Differential Charging*. The fluxes of charged particles can charge some parts of a spacecraft to a greater extent than others. This can lead to large electrical discharges across the satellite. The damage caused by such effects can be limited by careful design of the spacecraft surface.

(ii) *Single Events Upsets* (SEUs). Particles producing ionisation inside the satellite electronics can cause a malfunction. These are often 'soft' failures in that they can be cured by re-loading the corrupted on-board software.

(iii) *Latch-ups.* These are SEUs that lead to unwanted currents, which may also cause 'hard' failures in which satellite electronics are irreparably damaged. These can be minimised by good spacecraft design, which limits the extent of the unwanted current loops.

(iv) *Ionisation Effects in Microelectronics Components.* Energetic particles ionise within the semiconductor devices, and the currents that flow as a result can cause damage by ohmic heating and lattice degradation. This problem is getting worse in that the size of the devices, relative to the width of an ionisation trail, is decreasing. Smaller devices save weight and power (and thus reduce launch costs) and reduce the numbers of failures due to frozen solder joints. However, they are also much more susceptible to ionisation effects. Advanced warning of dangerous fluxes of ionising particles would allow the voltages to be switched off so that the ionisation does not lead to the destructive currents.

(v) *Deep Dielectric Charging.* Exposure to persistent fluxes of HREs causes a gradual build-up of free charge in insulators (thermal control blankets, cables, electronic boards, insulators, etc.). When these build up faster than they can leak away, there can be a highly damaging discharge event.

(vi) *Orbit Decay.* Particle precipitation in the auroral ovals helps enhance the electrojet currents, which give global heating of the upper atmosphere. This raises the concentration at a given height and increases the frictional drag on the satellite, causing it to fall to a lower altitude.

All of the above effects increase and decrease in both frequency and severity with the solar cycle. Sunspots are now rising in the 23rd cycle of sunspots seen since records began [Kunches, 1998], and failures are beginning to occur. It is not yet clear how active the Sun will be at the peak of this cycle (due around 2001), but it is clear that modern satellites are more vulnerable to the effects of the particle radiations and that society is more reliant on them than ever before. In January 1997, the satellite-TV craft Telstar 401 failed during the impact of a coronal mass ejection which had been tracked from the Sun to the Earth by the SOHO satellite [Reeves *et al.*, 1998]. More recently, there was a storm in May 1998 which has been linked to the demise of two satellites and a malfunction of a third [Baker *et al.*, 1998]. The satellites that failed were EQUATOR-S (a scientific satellite, ironically, designed to study the STP effects that almost certainly led to its demise) and Galaxy 4, a geostationary communications satellite. The loss of the latter caused widespread disruption to communications and the loss of a pager service to no less than 45 million customers. The attitude control system on the satellite failed on 19 May, two weeks after a major storm disturbance, which was followed by exceptionally high fluxes of HREs over a prolonged period. This appears to have been a classic example of the destructive effect of deep dielectric charging.

The top panel of Figure 2 shows this storm in May 1998, as seen in the 14-day running means of the planetary geomagnetic Ap index for April/May 1998 (note that Ap is very similar to the Kp index shown in Figure 1). Large values, with daily means exceeding 25 nT, were seen for 12 days. To put this in context, the daily means of Ap had only rarely risen above 10 nT, and never above 15 nT, in the previous year. The 14-day integrated fluxes of 3·5–6·0 MeV electrons, seen at geostationary orbit by the Los Alamos National Laboratory satellite LANL 1994–084, rose to more than three
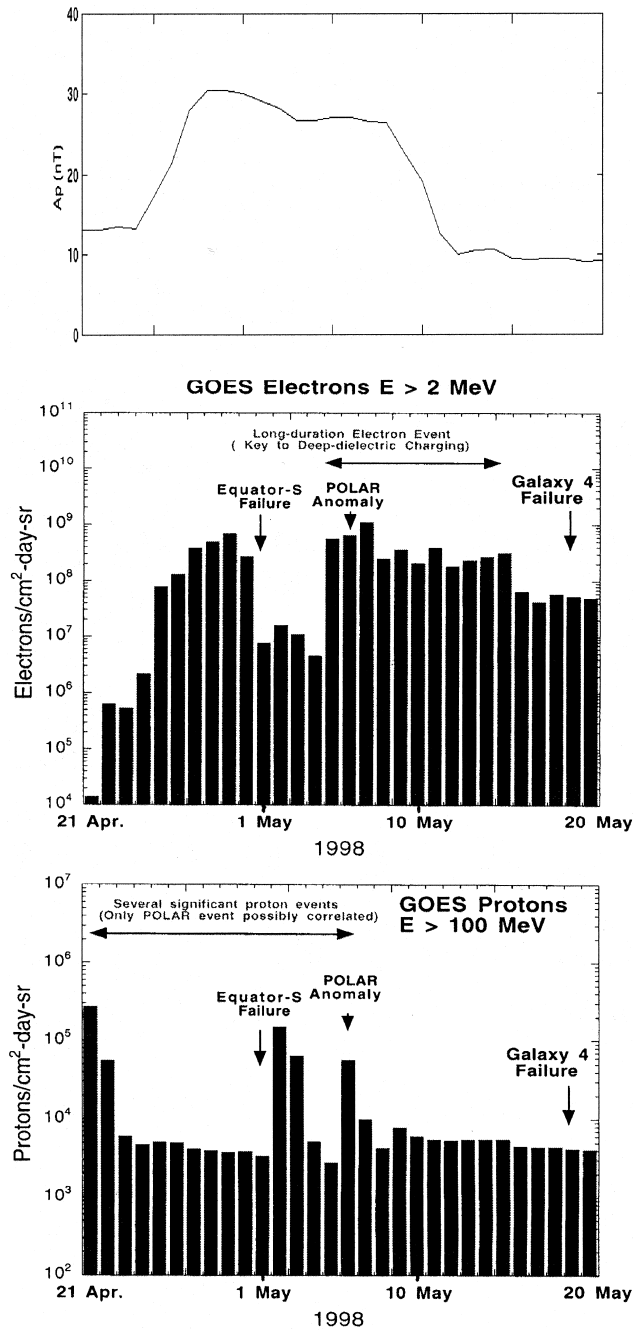
Figure 2. Daily means of the planetary geomagnetic index, Ap for 21 April to 20 May 1998 (top) and fluxes observed by GEOS of > 2 MeV electrons (middle) and > 100 MeV protons (bottom). The dates on which three spacecraft encountered operational problems are marked [from Baker *et al.*, 1998].
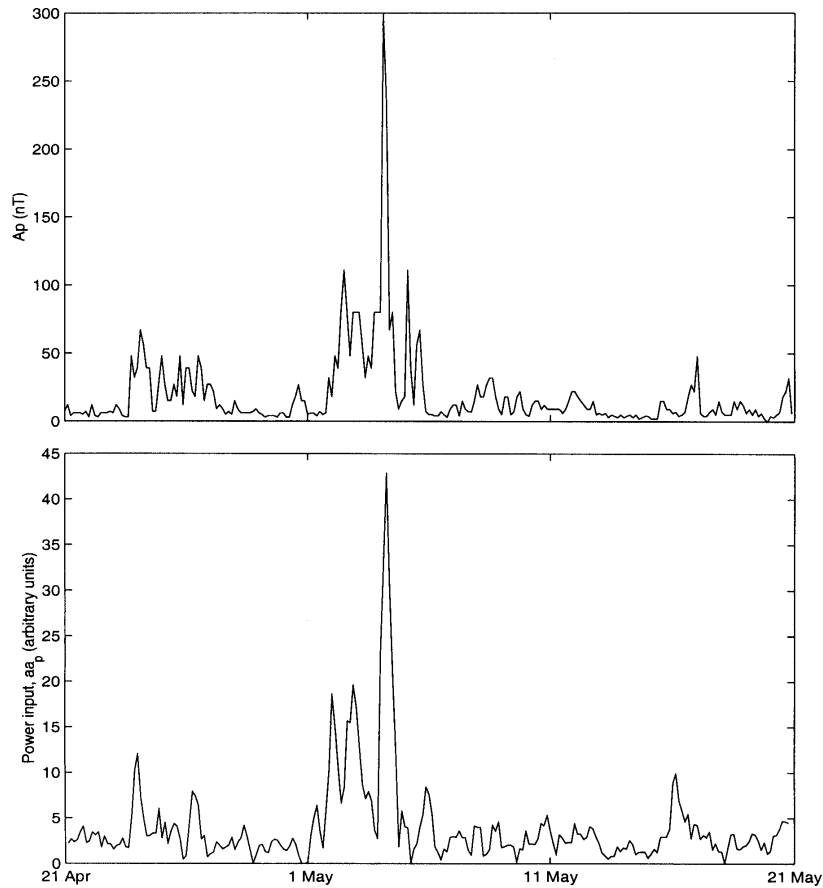
Figure 3. Analysis of the major storm commencing on 2 May 1998 (see Figure 2): (top) the observed geomagnetic index Ap; (bottom) the predicted power input to the magnetosphere, P_m, using the best-fit coupling function derived by Stamper et $al.$ (1998).

times the levels detected previously in the year, with smaller fractional rises also seen at lower energies [Baker et $al.$, 1998]. The middle panel of Figure 2 shows the daily means of fluxes of > 2 MeV electrons seen during this storm by another geostationary satellite GOES, and the bottom panel shows the daily means of the fluxes of > 100 MeV protons. Also marked are the dates on which three spacecraft encountered operational problems.

Figures 3 and 4 show the conditions in the magnetosphere and interplanetary space that led to this storm. The top panel of Figure 3 shows the unsmoothed 3-hourly Ap index values, which briefly peak at 300 nT. The second panel shows the power input to the magnetosphere, estimated from the measured solar wind flow and interplanetary magnetic field, P_m, using the best-fit formulation by Stamper et $al.$ (1998):

$$P_\mathrm{m} = (1\cdot8572 \times 10^{-17}) \langle M_\mathrm{E} \rangle^{2/3} \langle N_\mathrm{sw} \rangle^{0\cdot32} \langle v_\mathrm{sw} \rangle^{1\cdot63} \langle B_\mathrm{sw} \rangle^{0\cdot70} \langle \sin^4(\theta/2) \rangle, \qquad (1)$$

where M_E is the Earth's magnetic moment in T m³, N_sw is the solar wind concentration in m⁻³, v_sw is the solar wind velocity in km s⁻¹, B_sw is the IMF magnitude in nT and
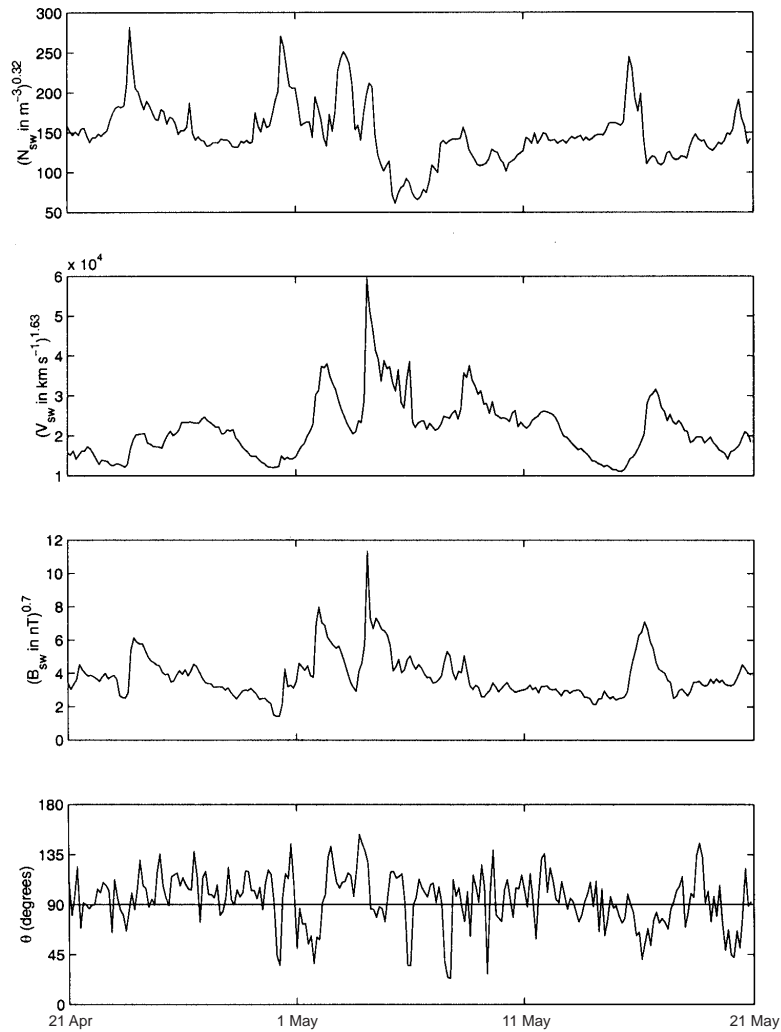
Figure 4. The variations of three-hour averages of the terms in the predicted power input, P_m as observed by the WIND satellite (from top to bottom): $\langle N_{sw} \rangle^{0.32}$, $\langle v_{sw} \rangle^{1.63}$, $\langle B_{sw} \rangle^{0.70}$, and $\langle \theta \rangle$ (see text for details). Data courtesy of K. Ogilvie and R. Lepping.

θ is the clock angle that the IMF makes with the northward direction in the Earth's GSM magnetic frame of reference. This best-fit estimate of the power input to the magnetosphere was derived using the theoretical formulation established by Vasyluinas *et al.* (1982). It can be seen that the agreement is remarkably good. In the lower panel, six-hour means of P_m are employed. It is found that geomagnetic indices like Ap (or Kp) and *aa* are well correlated with P_m on time scales from years down to about six hours. However, on shorter time scales, the characteristic substorm response time of the magnetosphere becomes important and the correlation begins to break down.

The storm followed the impact of a CME, but its development was also influenced by solar flares and high speed solar wind flow streams. Figure 4 shows the various terms that enter into the predicted power input. The solar wind concentration N_{sw},
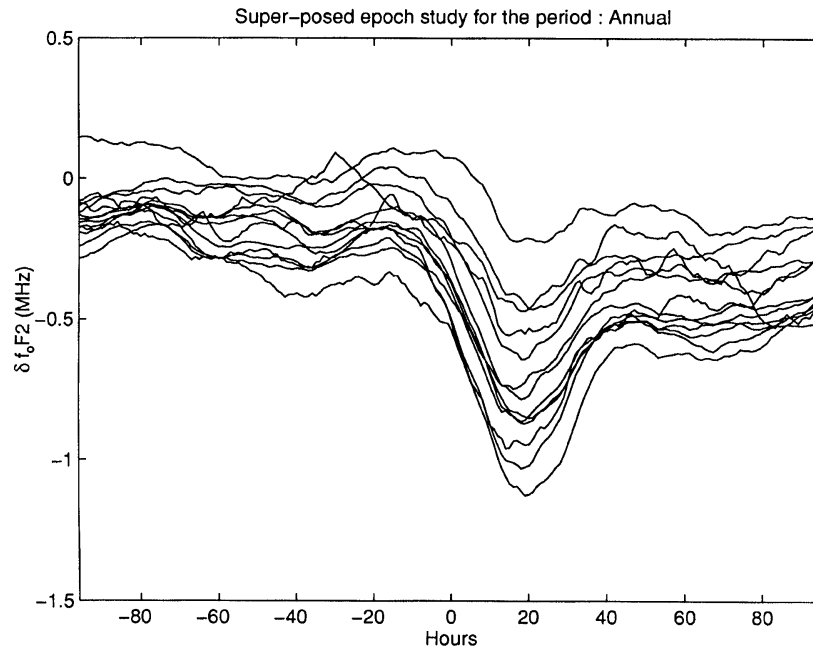
Figure 5. Superposed epoch plots of storm-time ionospheric perturbations (as in Figure 1*f*), for European ionospheric stations between northern Scandinavia and the Mediterranean. Deviations of the F-layer critical frequency from quiet time values, δfoF2, is shown as a function of time relative to a major southward IMF turning ($\Delta B > 11\cdot 5$ nT, at time zero) [from Wild *et al.*, 1998].

was relatively high; however, it was the combination of exceptionally high solar wind speed v_{sw}, (peaking at 800 km s^{-1}), high IMF (B_{sw} near 16 nT) and a southward IMF orientation (θ above 90°) that produced such a large and destructive event. These values can be compared with the occurrence distributions over three solar cycles given by Hapgood *et al.* (1991) – for example the solar speed is above the upper decile. However, what is extreme is the combination of these unusual values.

The severity of these effects on spacecraft depends on a number of factors, including the spacecraft design, construction and orbit. GPS satellites are constructed to standards that make them amongst the most robust in space, borne out by their exceptionally low failure rate. Achieving this longevity requires the use of radiation-hardened electronics, duplication and shielding, with consequent penalties in launch weight, power requirements and cost. In addition, the orbit of GPS satellites does not take them through the regions of greatest radiation hazard on a regular basis, unlike Geostationary and Geostationary Transfer Orbits.

3. GLOBAL IONOSPHERIC STORMS. The currents that flow in the auroral ionosphere that cause the increase in the Ap and Kp indices also deposit energy in the neutral upper atmosphere (the *thermosphere*). This heating causes an upwelling of molecular gases and enhanced winds away from the auroral oval. Both influence the ionosphere at all latitudes, giving an *ionospheric storm* following major energy input from the solar wind. The winds blow ionospheric plasma up field lines to where the loss rates are lower – as a result ionospheric concentrations and *total electron content* (TEC) can increase (called a positive phase of the storm) [Ho *et al.*, 1996]. However, the enhanced winds also bring the molecular-rich gas from the
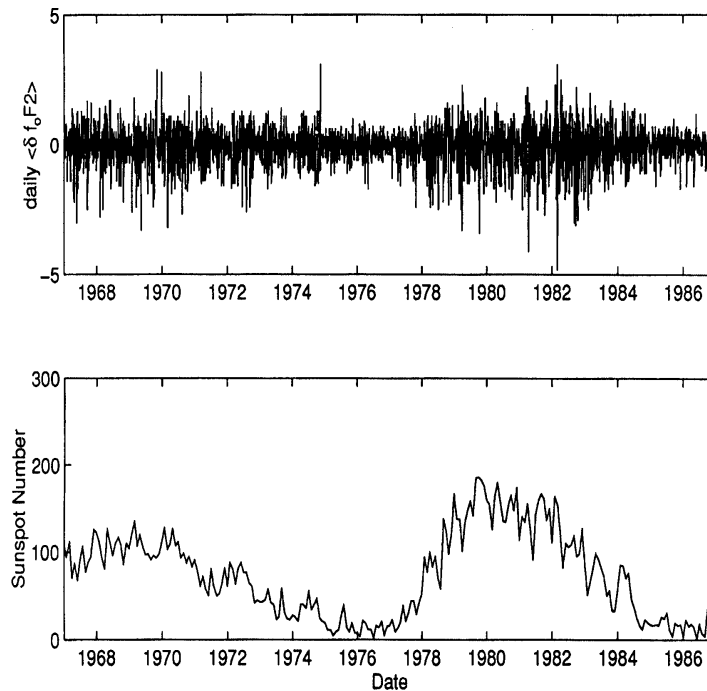
Figure 6. (Top) Daily averages of the ionospheric perturbation of the F2-layer critical frequency from quiet-time values, δfoF2, as observed by the Slough ionosonde during 1967–1987. (Bottom) The sunspot numbers. Negative values of δfoF2 correspond to depletions of the ionosphere and are largest in the main phase of ionospheric storms [from Wild *et al.*, 1998].

auroral ovals to lower latitudes, and this reduces the ionospheric concentrations and TEC (giving the subsequent negative or main phase to the storm). We now have global numerical models of the mutually coupled ionosphere – thermosphere system that can model and predict these effects [e.g. Millward *et al.*, 1995]. Figure 5 shows the superposed epoch plots of the mean change in the F-region critical frequencies, δfoF2, following a south-ward turning of the IMF at time zero (like Figure 1f). Each line is for one of a number of different ionosonde stations in Europe, between northern Scandinavia and the Mediterranean. The changes are simultaneous at all latitudes but weaker for the lower latitude stations. At lower latitudes the negative phases (negative δfoF2) are more likely to be preceded by a positive phase (positive δfoF2).

The top panel of Figure 6 shows the daily means of δfoF2 for the Slough ionosonde between 1967 and 1987. The lower panel shows the sunspot numbers for comparison. It can be seen that the large ionospheric disturbances (both positive and negative disturbances) are seen at larger sunspot numbers.

These ionospheric storms cause a variety of effects to a variety of navigational systems:

(i) The variations in TEC affect the phase of signals propagated through the ionosphere and introduce group delays to the propagation time of pulses. As a result, GPS receivers using a single frequency are subject to considerable positioning errors.
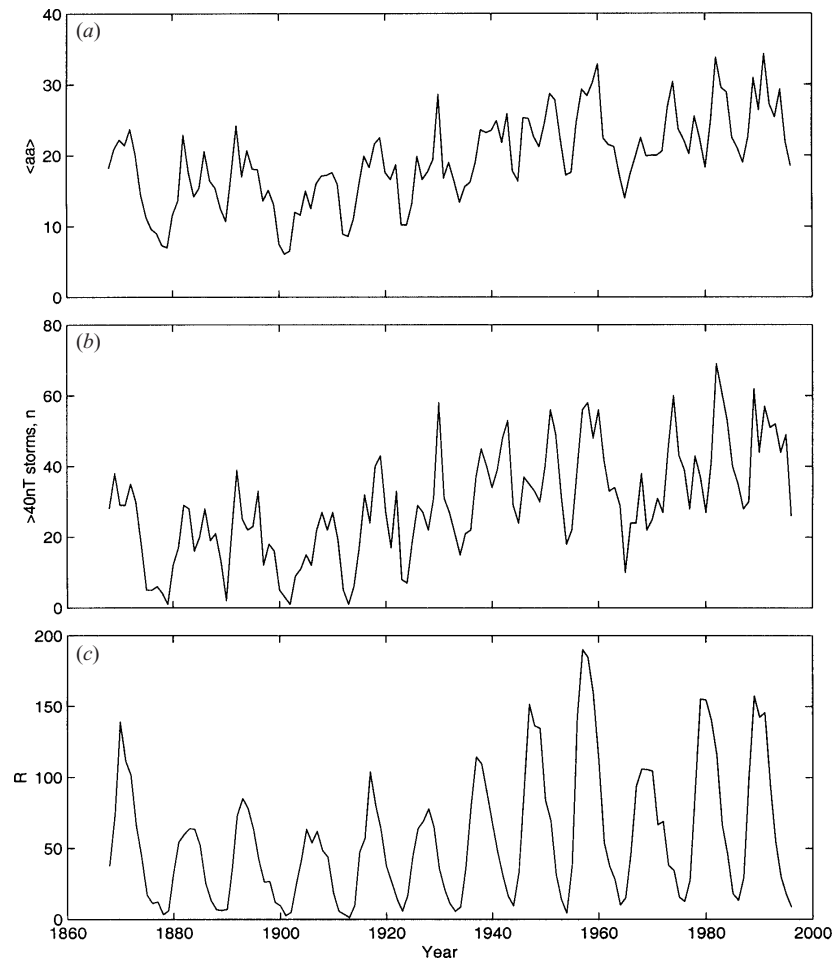
Figure 7. (*a*) Annual means of daily *aa* values, $\langle aa \rangle$; (*b*) number of storms (*aa* > 40 nT) per year, *n*, and (*c*) the smoothed sunspot number, *R* for 1868–1996.

(ii) The problem of TEC changes and GPS position errors is largely solved by using dual-frequency systems. However, irregularities in the ionosphere are also more prevalent during storms and these give rise to phase and amplitude *scintillations* of the signals which can give problems.

(iii) The ionospheric depletion during storms reduces the range of frequencies available to HF systems, including over-the-horizon radars. In addition, such radars suffer positioning errors as propagation paths in the ionosphere are altered.

(iv) The low-altitude ionisation produced by X-rays and energetic particles from flares give rise to errors in positioning by the Loran-C system which can become sufficiently severe that the system cannot be used.

4. LONG-TERM TRENDS. We have learned much in recent years about how the solar disturbances influence the Earth's space environment and the navigation systems that operate within it. As yet we cannot accurately forecast the effects of

individual events or 'space weather', even though we know about the statistics of events (equivalent to the climate in space). However, there is recent evidence for long-term changes in the Sun causing long-term changes in the magnetosphere and ionosphere [Stamper *et al.*, 1998]. The top panel of Figure 7 shows the annual mean values of the geomagnetic activity, as quantified by the *aa* index, which was retrospectively compiled back to 1896 by Mayaud (1972). On these annual time scales *aa* is very well correlated with the other planetary geomagnetic indices, Ap and Kp, and with the auroral electrojet index, AE. The middle panel of Figure 7 shows the number of storms per year during which *aa* exceeds 40 nT and the lower panel shows the sunspot numbers. It can be seen that all three are well correlated, showing strong solar cycle variations. Notice that geomagnetic activity lags behind the sunspot numbers because fast solar wind streams, and the associated recurrent storms, are mainly seen in the declining phase of the sunspot cycle. However, Figure 7 also shows that there are long-term changes in all three of these parameters. In particular, geomagnetic activity has gradually increased throughout this century, apart from a drop around the time of the start of solar cycle 20 (i.e. around 1964). That the same behaviour can be seen in the sunspot numbers, strongly suggests that this drift is due to changes in the Sun.

Since 1964, we have monitored the solar wind in interplanetary space and recently Stamper *et al.* (1998) have used these data to show how the Sun has changed. They derived the best-fit estimate to the power input to the magnetosphere, P_m, as given by equation (1) in section 2. The annual means of P_m and *aa* for 1964–1996 are shown in Figure 8. The fit is least good early in the data sequence, possibly because there are
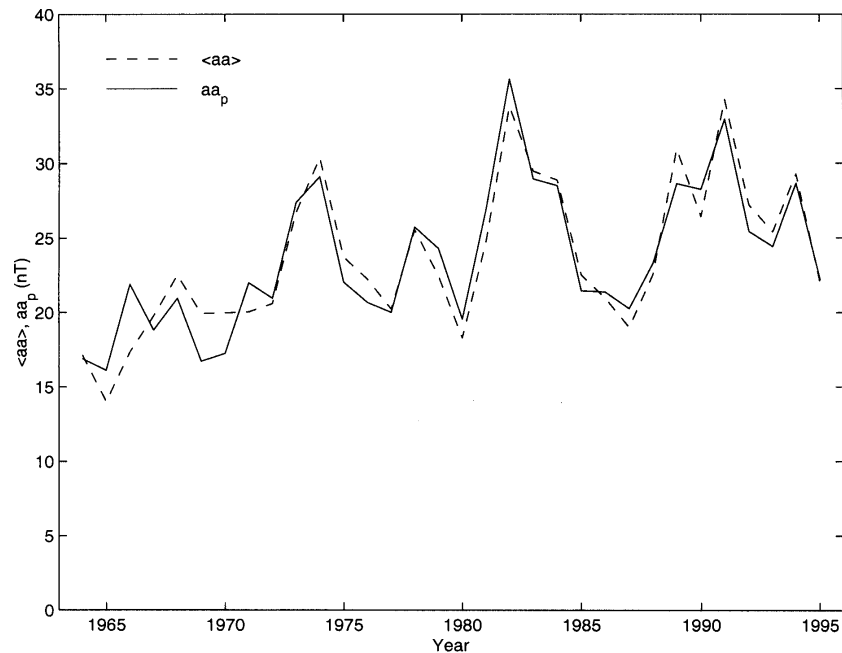

Figure 8. Annual means of the geomagnetic *aa* index (dashed line) and of the power input to the magnetosphere, P_m (solid line) for solar cycles 20, 21 and 22 (1964–1996) [from Stamper *et al.*, 1998].

some uncertainties about the calibration of the space measurements for these early data. Even so, the correlation coefficient is 0·95 which is virtually significant at the 100 % level (the probability of reaching this result by chance is 10^{-16} %!). This extremely good correlation is very valuable because we can analyse the factors in equation (1) and so understand more about the variations of the power input to the magnetosphere. Because the data cover three full sunspots cycles, the authors were able to identify the causes of the drift in geomagnetic activity by analysing the long-term drift in the various terms in equation (1). They showed that the decrease in the Earth's magnetic moment and the fact that the IMF has increasingly tended to lie in the ecliptic plane are two effects that have acted to reduce the rise in geomagnetic activity, such that the terms $\langle M_{\mathrm{E}} \rangle^{2/3}$ and $\langle \sin^4(\theta/2) \rangle$ showed percentage rises of $-1·7$ % and $-9·3$ %, compared to the overall rise in the aa index of 39 % over the period 1964–1996. It was also shown that the drift in the orientation of the Earth's magnetic axis did not contribute to the change. The main factors in the rise in aa were a 17·5 % rise in $\langle B_{\mathrm{sw}} \rangle^{0·70}$, a 15·3 % rise in $\langle N_{\mathrm{sw}} \rangle^{0·32}$ and a 11·9 % rise in $\langle v_{\mathrm{sw}} \rangle^{1·63}$. Thus the upward trend in geomagnetic activity since 1964 has been due to increases in the concentration and speed of the solar wind seen at Earth and in the magnitude of the IMF. The last of these three has the largest effect, and Stamper et al. (1998) have shown that it is due to a gradual increase in the total open flux of the Sun that emerges into interplanetary space through the coronal holes (which has increased by 33 % during solar cycles 20, 21 and 22). This is a very significant finding, and the next step is to understand why this has occurred. Only then will we be able to extrapolate the data sequences shown in Figure 7 into the future and so predict our space climate over the next few solar cycles.

5. SUMMARY. The near-Earth magnetosphere, the ionosphere and the upper atmosphere are sometimes collectively referred to as '*Geospace*'. The variations in geospace have great implications for both satellite and terrestrial navigation systems. In particular, satellite failures, GPS positioning errors, HF radar blindness and bearing errors will all undoubtedly become increasingly serious problems in the next few years with the increased sunspot numbers of the current solar cycle. Modern spacecraft technology may prove to be particularly at risk during the next maximum of geomagnetic activity, due around the year 2001. All these effects are caused by energy that is extracted from the solar wind flow by the Earth's magnetic field by the process of magnetic reconnection. We now understand a great deal about this energy transfer and, in particular, the role of solar features (such as coronal mass ejections and fast streams from low-latitude coronal holes) in generating storms in geospace. Thanks to long-term monitoring of geospace, we are only now beginning to learn about changes in the Sun and how they might affect our operational systems in the future.

REFERENCES

Baker, D. N., Allen, J. H., Kanekal, S. G. and Reeves, G. D. (1998). Disturbed space environment may have been linked to pager satellite failure, EOS, Trans. Am. Geophys. Union, 79 (40), 477–483.

Cliver, E. W., Boriakoff, V. and Bounar, K. H. (1996). The 22-year cycle of geomagnetic activity. *J. Geophys. Res.*, **101**, 27091–27109.

Davis, C. J., Wild, M. N., Lockwood, M. and Tulunay, Y. K. (1997). Ionospheric and geomagnetic response to changes in IMF Bz: a superposed epoch study. *Annales Geophys.*, **15**, 217–230.

Fox, N. J., Peredo, M. and Thompson, B. J. (1998). Cradle to grave tracking of the January 6–11, 1997 Sun–Earth connection event. *Geophys. Res. Lett.*, **25**, 2461–2464.

Hapgood, M. A., Bowe, G., Lockwood, M., Willis, D. M. and Tulunay, Y. (1991). Variability of the interplanetary magnetic field at 1 A.U. over 24 years: 1963–1986. *Planet Space Sci.*, **39**, 411–423.

Ho, C. M., Mannucci, A. J., Lindqwister, U. J., Pix, X. and Tsurutani, B. T. (1996). Global ionosphere perturbations monitored by the world-wide GPS network. *Geophys. Res. Lett.*, **23**, 3219–3222.

Joselyn, J. A. (1995). Geomagnetic activity forecasting: the state of the art. *Rev. Geophys.*, **33**, 383–401.

Kunches, J. M. (1998). The rise of solar cycle 23 and navigation systems. *Proceedings*, *NAV98*, International Conference of the Royal Institute of Navigation, London, paper 14.

Lockwood, M. (1997). Cluster's last stand? *Astron. and Geophys.*, **38** (1), 21–25.

Mayaud, P. N. (1972). The *aa* indices: a 100-year series characterising the magnetic activity. *J. Geophys. Res.*, **72**, 6870–6874.

Millward, G. H., Rishbeth, H., Fuller-Rowell, T. J., Aylward, A. D., Quegan, S. and Moffett, R. J. (1996). Ionospheric F2-layer seasonal and semi-annual variations. *J. Geophys. Res.*, **101**, 5149.

Reeves G. D. *et al*. (1998). The relativistic electron response at geosynchronous orbit during the January 1997 geomagnetic storm. *J. Geophys Res.* (in press).

Stamper, R. Lockwood, M., Wild, M. N. and Clark, T. D. G. (1998). Solar causes of the long-term increase in geomagnetic activity. *J. Geophys. Res.* (submitted).

Vasyluinas, V. M., Kan, J. R., Siscoe, G. L. and Akasofu, S.-I. (1982). Scaling relations governing magnetospheric energy transfer. *Planet Space Sci.*, **30**, 359–365.

Wang, Y.-M., Hawley, S. H. and Sheeley, N. R. Jr. (1996). The magnetic nature of coronal holes. *Science*, **271**, 464–469.

Webb, D. F. and Howard, R. A. (1994). The solar cycle variation of coronal mass ejections and solar wind mass flux. *J. Geophys. Res.*, **99**, 4201.

Wild, M. N., Lockwood, M., Stamper, R., Davis, C. and Tulunay, Y. (1998). Ionospheric disturbances following southward turnings of the IMF. *Annales Geophys.* (to be submitted).

KEY WORDS

1. Space Weather.   2. Navaids.   3. Satellites.   4. Safety.